# Supporting Information

Sahl et al. 10.1073/pnas.0912894107

## SI Text

**Materials.** ***Supported lipid bilayer (SLB).*** Lipid bilayers were prepared based on the procedure described by Chiantia et al. (1). Briefly, the lipid DOPC (1,2-dioleoyl-sn-glycero-3-phosphocholine) and the fluorescent lipid (PE) analog were mixed in organic solvents (Chloroform/MeOH 3:1) at a lipid concentration of ~10 mg/mL. The concentration of the fluorescent lipid analogs was on the order of $10^{-4}$ mol%. We evaporated 50 μL of the lipid stock solution for 30 min under vacuum. The dry lipid film was slowly rehydrated with 50 μL buffer solution (150 mM NaCl, 10 mM Hepes) and resuspended by vigorous vortexing. A small aliquot (10 μL) of the suspension was further diluted in 140 μL of the same buffer solution and sonicated for 30 min at 35 °C until the buffer-lipid solution had become transparent. This solution was filled into a microscopy chamber and a small amount of $MgCl_2$ (to an end concentration of 3 mM) was added to force vesicle spreading and to initialize the bilayer formation. 30 min later, the sample was thoroughly rinsed and kept under buffer solution. Such bilayers were stable for several hours.

***Cell culture.*** The epithelial cell line PtK2 was grown as described previously (2). For further treatment, the cells were seeded on standard glass coverslips to a confluence of about 80%. The cells were grown at 37 °C in a water-saturated atmosphere of 5% $CO_2$ in air. All media and supplements were purchased from Invitrogen.

***Membrane incorporation of fluorescent lipid analogs.*** The incorporation of the fluorescent lipid analogs was performed as described in ref. 2. In summary, complexes of the labeled lipids and Bovine Serum Albumin (BSA) were prepared according to Martin and Pagano (3) and Schwarzmann et al. (4) with slight modifications. In brief, 100 nmol of the lipid stock solutions ($CHCl_3$/MeOH, 3:1) were dried under a stream of nitrogen. The dried lipids were dissolved in 20 μL of absolute ethanol and vortexed vigorously after addition of 1 mL of defatted BSA solution (100 μM, i.e., $10^{-4}$ M defatted BSA in Dulbecco's Modified Eagle Medium DMEM without phenol-red buffered with 10 mM Hepes). Addition of 9 mL HDMEM (Hepes + DMEM) resulted in a final concentration of 10 μM BSA and 0.2% ethanol. In the case of PE the BSA concentration was twice as large ($2 \times 10^{-4}$ M). Subsequently, cells were washed with HDMEM and incubated with BSA-lipid-complexes on ice for 30 min, then washed in cold HDMEM and incubated at 37 °C for 4 min in HDMEM. We incubated with varying concentrations of BSA-lipid-complexes in order to achieve suitable densities of the labeled species in the plasma membrane.

***Treatment with cholesterol oxidase (COase).*** To modify the cholesterol content of the plasma membrane, cells were treated with 1 U/mL *Streptomyces spec*. cholesterol oxidase (COase, Sigma, stock solution 34 U/mL in 50 mM $KH_2PO_4$, pH 7.5) in HDMEM for 30 min at 37 °C, before being washed in HDMEM. The COase treatment was performed just before the insertion of the fluorescent lipid analogs into the plasma membrane. Values extracted from COase treated cell measurements vary more strongly due to an additional variation of the degree of cholesterol depletion by COase. Three measurements which showed no effect after COase treatment were excluded from further analysis.

***Measurements.*** We analyzed the lipid dynamics in the lower plasma membrane facing the coverslip and completed all measurements before significant internalization or any morphological changes in the cell could take place. We performed most measurements at room temperature (22 °C–23 °C). Previous experiments showed that the overall lipid dynamics do not change in this temperature regime, except a slight slowdown of free diffusion (2). Lipid internalization and cholesterol recovery after COase treatment is faster at 37 °C, which would leave a smaller time window for sufficient measurements compared to 23 °C. We excluded diffusion of nonintegrated lipids by control measurements in between the cells.

**Controls.** ***Potential influence of the fluorophore.*** Any fluorescence microscopy or nanoscopy technique uses fluorescent probes. These probes may influence the properties of the labeled molecules. Therefore, it is important to perform control experiments ruling out as much as possible that the observed behavior of the fluorescent analogs is dissimilar to their native diffusion in membranes. Details of various controls can be found in the Supplements to ref. 2, where potential influences on the lipid dynamics due to, e.g., the dye labeling position, the degree of polarity of the dye label, the dye structure or the membrane affinity of the fluorescent lipid analog are discussed in detail.

Here we made an additional control experiment: Replacing the acyl-chain-labeled sphingolipid analog SM by the headgroup-labeled variant CPE showed no significant difference in our fast tracking experiments ($\alpha \approx 0.35$, $D \approx 0.25$ μm$^2$/s, $r_{trap} \approx 5$ nm, $\bar{t}_{trap} \approx 20$ ms for CPE (6 measurements, standard deviations ~10–30%) compared to $\alpha \approx 0.35$, $D \approx 0.35$ μm$^2$/s, $r_{trap} \approx 5$ nm, $\bar{t}_{trap} \approx 17$ ms for SM).

***Photobleaching and averaging effects.*** Large excitation powers may result in enhanced photobleaching, especially in case of lipids being trapped during tens of milliseconds (5). Photobleaching would result in an overestimation of the (time-)fraction α of the free diffusion regime. We have performed several controls to ensure that the applied laser power of ~5–20 μW (i.e., focal intensity of ~5–20 kW/cm$^2$) for fluorescence excitation did not induce significant photobleaching and did not bias our analysis.

1. Plotting the first and last points localized for ~20,000 trajectories of SM in living cells (recorded for ~15–20 μW) shows that most points reside on the periphery (Fig. S4). However, as a result of the burst selection criteria, some of the entering molecules are first localized well on their way towards the center and some will not leave the observation area at the very edge. Comparing the number of nonperipheral localizations upon entry and exit of fluorophores reveals that about 2–3% of them are photobleached during the transit; i.e., the influence of photobleaching is sufficiently small for a bias-free statistical analysis of molecular diffusion and transient trapping.
2. Stemming from the shortened observation time, in FCS, photobleaching leads to a shortening of the correlation curve (5). FCS data recorded for SM diffusion in living cells (Fig. S6*A*, recorded for ~15 μW) reveals an average transit time of 30 ms, which is in line with the transit times through the confocal spot measured in our previous STED-FCS experiments (2, 5), where we have as well performed several tests to exclude a notable influence of photobleaching.
3. Last but not least, single-molecule tracking data of SM in living cells recorded at 5–10 μW compared to 15–20 μW exhibited no decrease of the (time-) fraction α of the free diffusion regime, as would be expected for a significant influence of photobleaching at larger power levels. Instead, values of α

increase from ~0.35 at 20 μW, ~0.5 at 10 μW to ~0.6 at 5 μW for windows of $N = 250$ photons. At 5–10 μW the count rate per molecule $Q$ is reduced and the temporal resolution $\Delta t = N/Q$ is lowered, which degrades the ability to discern short trapping events from free diffusion. Therefore, the apparent (time-)fraction α of the free diffusion regime increases. This is a general challenge of single-molecule tracking experiments (6) and the reason why often bright but large signal markers such as gold particles or quantum dots are applied (6–10). Our chosen excitation powers of 15–20 μW provide sufficient time resolution while keeping the influence of photobleaching still negligible. Our final values of α represent upper bounds and we can be confident that trapping is present to at least the measured degree and that the distinct differences between SM and PE diffusion do exist.

**Analysis.** ***Summary of the analysis procedure.*** Our single-molecule tracking analysis resulted in the physical characterization of lipid diffusion in a given system by extracting the diffusion constant $D$, the time-fraction of free diffusion α and an estimate of the radius $r_{\mathrm{trap}}$ of the trapping area. The analysis programs were implemented in MATLAB, with a few subroutines in C++ . The analysis steps were as follows.

- For each detected photon $i$ we recorded a value pair $\{t_{ph,i}, \mathrm{chan}_i\}$ of the macroscopic time $t_{ph,i}$ (absolute time with respect to the start of the measurement) and of the channel number $\mathrm{chan}_i$ (detector number).
- The photon events were consecutively binned into windows of $N = 250$ (or 1,000) photons, and the windows were advanced in steps of 25 (or 100) photons. A set of four parameters $\{t_j, I_j, x_j, y_j\}$ was obtained for each photon window $j$: the macroscopic time $t_j$ is the average time $\langle t_i \rangle$ of the macroscopic times $t_i$ of all $N$ included photons; the average signal intensity $I_j = N/(t_N - t_0)$ (where $t_0$ and $t_N$ are the macroscopic times before the first and of the last included photon, respectively); and the spatial position $(x_j, y_j)$ determined from three photon count values $S_1$, $S_2$ and $S_3$ in channels 1 to 3. This triple $(S_1, S_2, S_3)$ is compared to the reference map to find the coordinates $(x_j, y_j)$ where it best matches the reference triple $\{(R_1, R_2, R_3)\}$ encoding the relative detection efficiencies. The best agreement of $(S_1, S_2, S_3)$ with respect to $\{(R_1, R_2, R_3)\}$ is determined by a maximum-likelihood scheme.
- The bursts (i.e., molecular transits) were identified as those elements of $\{t_j, I_j, x_j, y_j\}$ for which $I_j > \mathrm{threshold} = 5 \cdot B + 5 \cdot B/\sqrt{N}$, where $B$ is the uncorrelated offset signal (background) during the measurement, which was determined from the intensity distribution (see Fig. S6*B*).
- For each burst, the sequence of all positions within a confidence circle, i.e, within the central focal diameter of typically 240 nm make up the molecular trajectory $\vec{r}(t) = \{x_j, y_j\}(t_j)$.
- All statistically independent (nonoverlapping) mutual differences $\{\Delta r^2, \Delta t\}$ were calculated from $\vec{r}(t)$.
- Counting the numbers of $(\Delta r^2, \Delta t)$ falling within increments $\Delta(\Delta t) = 0.1$ ms and $\Delta(\Delta r^2) = 50\ \mathrm{nm}^2$ up to $\Delta t = 10$ ms yielded the probability density $p(\Delta r^2, \Delta t)$. Each count is weighted by the inverse intensity $1/I_j$, i.e., the time between adjacent localizations, to account for the variable time steps.
- Correcting of $p(\Delta r^2, \Delta t)$ by $1/P_{\mathrm{track}}(\Delta r, R)$ (see Fig. S7), cumulating and normalization along $\Delta r^2$ yielded the cumulative distribution $P(\Delta r^2, \Delta t)$.
- Global fit of

$$P(\Delta r^2, \Delta t) = \alpha\left[1 - \exp\left(\frac{-\Delta r^2}{4\sigma_r^2 + 4D\Delta t}\right)\right] + (1-\alpha)\left[1 - \exp\left(\frac{-\Delta r^2}{4\tilde{r}_{\mathrm{trap}}^2}\right)\right]$$

to the experimental cumulative distribution $P(\Delta r^2, \Delta t)$ yielded the diffusion constant $D$ of free Brownian motion, the time fraction α of free diffusion and the value $\tilde{r}_{\mathrm{trap}}^2$, which correlates with the spatial extent within which the lipids dwell during trapping (11, 12). $\sigma_r = 19$ nm is the experimental localization error of the live cell tracking experiments and has consistently been determined from free-running fits to all of the $P(\Delta r^2, \Delta t)$ data of the PE lipid. Probably due to the movement of the objects as well as due to some background, this value of $\sigma_r$ is slightly larger than $\sigma_r = 12.2$ nm determined from the fixed bead measurements (Fig. 2*D*). The values of $\tilde{r}_{\mathrm{trap}}^2$ allow an estimation of the radius $r_{\mathrm{trap}} = (\tilde{r}_{\mathrm{trap}}^2 - \sigma_r^2)^{1/2}$ within which molecules dwell during trapping.

The theoretical model (11, 12) is a superposition of (1) the solution to the diffusion equation (free Brownian diffusion, first term) and (2) a stationary solution (molecule trapped in fixed location, second term) with amplitudes α and $(1 - \alpha)$, respectively, i.e., strictly two regimes—mobile or stationary—are assumed and their relative presence in the molecular motion is identified.

The above steps constitute a "measurement," as for instance reported in Fig. 3*B*.

***Mean squared displacement.*** The mean squared displacement (MSD) was computed as the expectation value of the squared displacement $\langle \Delta r^2 \rangle$ for lag times $\Delta t$ from $p(\Delta r^2, \Delta t)$. The deviation from linear behavior starting at $\sim(95\ \mathrm{nm})^2$ (seen for SLB, Fig. 3*A*) is due to the finite area of observation ($R = 110$ nm in this case).

***Refined analysis of the spatial extent of trapping (magnifying analysis).*** We directly estimated the spatial extent of selected long traps. The underlying idea is that for free Brownian diffusion, as the lag time increases, it becomes increasingly unlikely that a molecule has not left a small circular domain. For a domain of diameter $d = 60$ nm more than 97% of all molecules will have left the domain after $\Delta t = 15$ ms by Brownian motion, given the known diffusion constant $D$ of the membrane lipids (alternatively, $\Delta t = 3.7$ ms for a $d = 30$ nm domain, for analysis of trajectories with $N = 1,000$ photons). Focusing on the spatial extent of long traps, we declared those instances where the lipid still resided inside the circular domain as transient traps and approximated the extent of the trapping area from the radial standard deviation $\tilde{r}^*_{\mathrm{trap}} = (\sigma_x \cdot \sigma_y)^{1/2}$ of the set of all localizations during this time.

Potential traps were identified by moving a circular subdomain of diameter $d$ (the "magnifying glass" domain) over the trajectories (step size $d/2$ in the $x$- and $y$-direction). Each time the criterion "lipid remains within the domain area $\pi(d/2)^2$ for longer than $\Delta t$" was satisfied, we recentered the circular subdomain in two iterations on the center of mass of the localizations, so as to ensure that the trap is roughly centered and that traps are not cut into parts. The standard deviation $\tilde{r}^*_{\mathrm{trap}} = (\sigma_x \cdot \sigma_y)^{1/2}$ of the present trap was then saved and its section of the trajectory excluded from further analysis to avoid multiple counting of the identical trapping event. Note that:

1. This analysis cannot claim any completeness; i.e., not all of the trapped events are identified (not even all instances where the lipid does dwell for longer than $\Delta t$ within the domain area $\pi(d/2)^2$, obviously shorter traps cannot be found as there is no way to disentangle them from normal Brownian motion).
2. Random localizations (without trapping) within a domain $\pi(d/2)^2$ would yield $\tilde{r}^*_{\mathrm{trap}} = d/4 = 15$ nm for $N = 250$ and 7.5 nm for $N = 1,000$, i.e., significantly above the value found for our traps. This indicates a true clustering of the localizations on the smaller length scale.

To determine the area on which the trapping interaction takes place, the mean values of $\tilde{r}^*_{\mathrm{trap}}$ were related to the localization

accuracy $\sigma_r^*$ of this refined analysis. An advantage of the magnifying analysis is that by concentrating only on trapped events it allows us to increase the number of photons used for spatial localization to $N = 1,000$ and thus to increase the localization accuracy. The value of $\sigma_r^*$ has been determined as the spread of 500 localizations of a stationary bead with the subdomain at the center of mass of the localizations, where each localization stems from photons within a 20 ms time window (i.e., a time on the order of our trap durations): $\sigma_r^* = 10.3$ nm ($N = 250$) and 4.2 nm ($N = 1,000$). We determined an average radius $r^*_{\mathrm{trap}} = (\tilde{r}^{*2}_{\mathrm{trap}} - \sigma_r^{*2})^{1/2}$ of the trapping area. Note that for the analysis with $N = 250$, it was not possible to extract $r^*_{\mathrm{trap}}$ as the average $\tilde{r}^*_{\mathrm{trap}}$ was even slightly lower than $\sigma_r^*$. Due to the greater number of photons $N$ employed, the localization accuracy of the magnifying analysis ($N = 1,000$) is higher and thus the values of the trap radius $r^*_{\mathrm{trap}}$ slightly smaller than the values of $r_{\mathrm{trap}}$ from the global fit analysis ($N = 250$).

The trajectories selected for this refined analysis represent the longest, most prominent traps, which potentially take up the largest area. This strongly suggests that the trapping occurs on the macromolecular scale.

Based on the set of traps identified as described above, we also histogrammed their duration and fitted the distribution with an exponential decay to obtain estimates of the characteristic trapping times $\bar{t}_{\mathrm{trap}}$.

***Definition of accuracies.*** Throughout this work, we applied the conventional definition of the standard deviation $\sigma$ of a distribution of $n$ values $x_i$: $\sigma = \left(\frac{1}{n-1}\sum_{i=1}^{n}(x_i - \bar{x})^2\right)^{1/2}$, where $\bar{x} = \frac{1}{n}\sum_{i=1}^{n} x_i$. In the case of normally distributed values the diameter of the distribution may be estimated by the full-width-at-half-maximum $\mathrm{FWHM} = \sigma\sqrt{(8 \ln 2)}$, which is the diameter of the area containing 50% of all localizations.


1. Chiantia S., Ries J., Kahya N. & Schwille P. (2006) Combined AFM and two-focus SFCS study of raft-exhibiting model membranes, *ChemPhysChem* 7:2409–2418.
2. Eggeling C. et al. (2009) Direct observation of the nanoscale dynamics of membrane lipids in a living cell. *Nature* 457:1159–1163.
3. Martin O.C. & Pagano R.C. (1994) Internalization and sorting of a fluorescent analogue of glucosylceramide to the Golgi apparatus of human skin fibroblasts: Utilization of endocytic and nonendocytic transport mechanisms. *J Cell Biol* 125:769–781.
4. Schwarzmann G., Hofmann P., Pütz U. & Albrecht B. (1995) Demonstration of direct glycosylation of nondegradable glucosylceramide analogs in cultured cells. *J Biol Chem* 270:21271–21276.
5. Ringemann C. et al. (2009) Exploring single-molecule dynamics with fluorescence nanoscopy. *New J Phys* 11:103054.
6. Fujiwara T., Ritchie K., Murakoshi H., Jacobson K. & Kusumi A. (2002) Phospholipids undergo hop diffusion in compartmentalized cell membrane. *J Cell Biol* 157:1071–1081.
7. Lessard G.A., Goodwin P.M. & Werner J.H. (2007) Three-dimensional tracking of individual quantum dots. *Appl Phys Lett* 91:224106(1–3).
8. Wells N.P., Lessard G.A. & Werner J.H. (2008) Confocal, three-dimensional tracking of individual quantum dots in high-background environments. *Anal Chem* 80:9830–9834.
9. Hellriegel C. & Gratton E. (2009) Real-time multiparameter spectroscopy and localization in three-dimensional single-particle tracking. *J R Soc Interface* 6:S3–S14.
10. McHale K., Berglund A.J. & Mabuchi H. (2007) Quantum dot photon statistics measured by three-dimensional particle tracking. *Nano Lett* 7: 3535–3539.
11. Schütz G.J., Schindler H. & Schmidt Th. (1997) Single-molecule microscopy on model membranes reveals anomalous diffusion. *Biophys J* 73:1073–1080.
12. Pinaud F. et al. (2009) Dynamic partitioning of a glycosyl-phosphatidylinositol-anchored protein in glycosphingolipid-rich microdomains imaged by single-quantum dot tracking. *Traffic* 10(6):691–712.


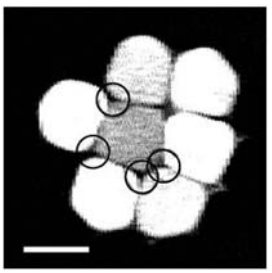

**Fig. S1.** Micrograph of fused fiber bundle. The central fiber is used in combination with two adjacent fibers. The small circles indicate some possible combinations. We highlight that our concept of the localization reference map, i.e., the encoding of the relative detection efficiencies as a function of the emitter position, readily deals with point-like detectors in almost arbitrary configurations. The fibers need not be equidistant from each other, although this is advantageous for a uniform localization accuracy. (Scale bar, 125 μm.)

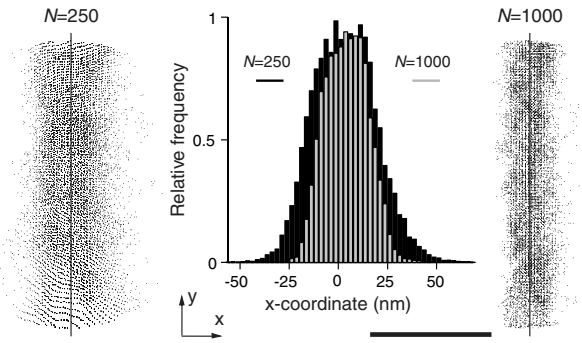


**Fig. S2.** Single 24 nm fluorescent beads scanned on a straight line through the observation region (82 transits) are adequately localized. The spread in the direction orthogonal to the transit is slightly higher than predicted from the stationary determination of the localization accuracy $\sigma_r$ (Fig. 2*D*), presumably as a result of small transverse oscillations induced by the scanning stage. (Scale bar, 100 nm.)

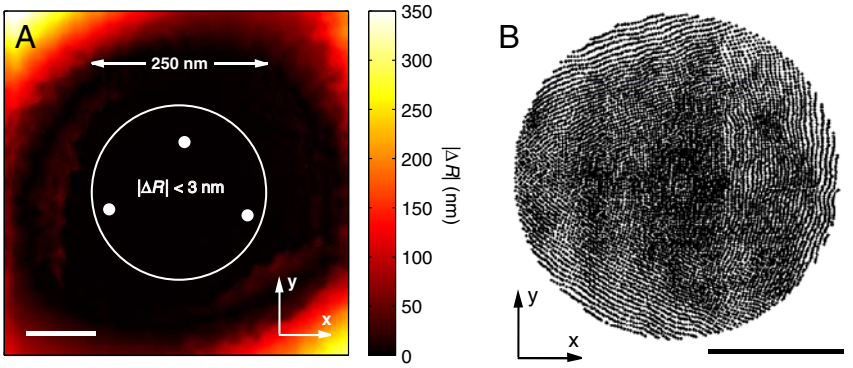


**Fig. S3.** Properties of the localization process. (*A*) Self-consistency of the localization map. By successively localizing each pixel element of the reference map through the maximum-likelihood scheme onto the identical map, followed by examining the displacement induced by this process, it became evident that the localization procedure has near-perfect fidelity. The systematic deviations $|\Delta R|$ in the central region of observation, to which analysis was limited, were ~3 nm or less. The white circles indicate the central positions of the three detection channels. (*B*) Example of >70, 000 localizations from lipid (PE) transits in living mammalian cells. The distribution on the map shows no discernible structure and is deemed uniform. (Scale bars, 100 nm.)

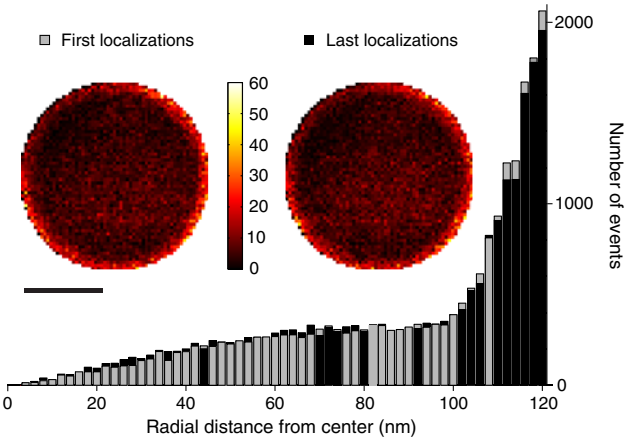


**Fig. S4.** Photostability of the fluorophore. The large majority of first and last points localized for ~20, 000 trajectories (SM lipids in living cells, excitation power of 15–20 μW) lie on the periphery (*Insets*). However, as a result of the burst selection criteria, some of the entering and leaving molecules are localized near the center. A slightly higher number left the observation area near the center. This small fraction (2–3%), most probably stemming from molecules lost from the observation due to irreversible photobleaching, is low enough to exclude a significant biasing effect of photobleaching on our single-molecule tracking data. (Scale bar, 100 nm.)

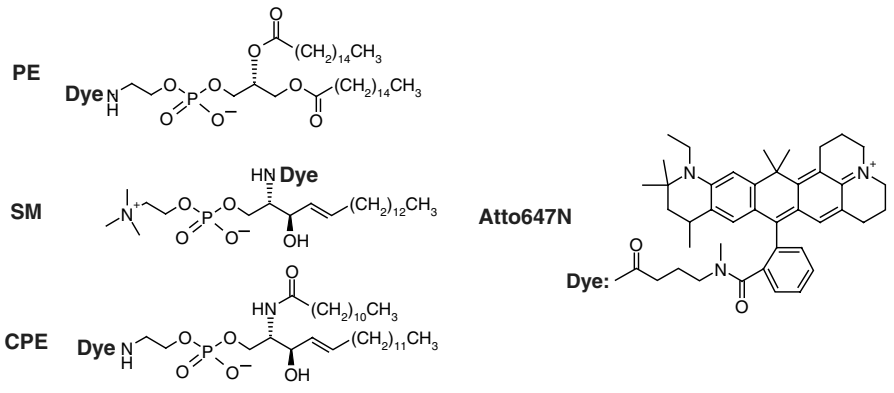


**Fig. S5.** Structural details of the different fluorescent lipid analogs and the lipophilic organic dye Atto647N. See *SI Text* for a discussion of controls and references pertaining to the potential influence of the dye label.

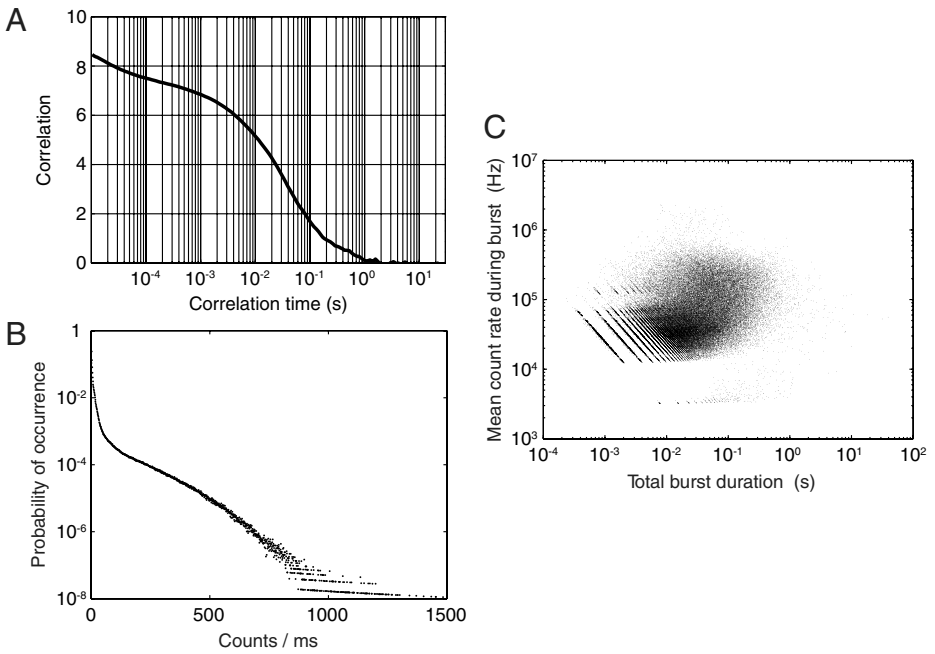


**Fig. S6.** Control of the true single-molecule measurement as required for the fast tracking method. (*A*) Typical auto-correlation (1) of a time-trace of single photon data from SM diffusion in the plasma membrane of living cells (excitation power of 15–20 μW). The characteristic diffusion time (~30 ms) is similar to previous measurements (2). The correlation amplitude demonstrates that the average number $M \approx 0.13$ of molecules in the focal volume is significantly below unity; i.e., the probability to detect more than one molecule at a time is very low (~1%) (3). (*B*) Probability distribution of photon counts of the same photon data. An analysis based on fluorescence intensity distribution analysis (FIDA) (4) results in $M \approx 0.07$ (i.e., a probability of 0.6% to detect more than one molecule at a time) and demonstrates an excellent signal-to-noise ratio of ~40 (averaged over all large and many small fluorescence bursts). While FIDA takes any background signal due to, for example, laser scattering into account, the background signal leads to a reduction of the correlation amplitude (5). Consequently, the value of $M$ determined by FCS is slightly larger than that determined by FIDA. (*C*) Scatter plot of the value pairs of burst brightness (mean count rate during burst) vs. burst duration for 109,417 lipid transits (PE, SM, SM-COase, CPE) in living cells. No significant signature of multimolecular events or events stemming from bright vesicles is observed, such events would be characterized by larger values of burst brightness. Note that the mean count rates shown here are obtained over the entire duration of the bursts, including the initial and final segments where the signal is small. For the central portion of trajectories [in the region of analysis (diameter of typically 240 nm), the count rates are higher and reach 600–1,000 kHz]. The pattern emerging for small value pairs of count rate and burst duration stems from the burst selection criteria.


1 Magde D, Elson E, Webb WW (1972) Thermodynamic fluctuations in a reacting system—Measurement by fluorescence correlation spectroscopy. *Phys Rev Lett* 29:705–708.
2 Eggeling C, et al. (2009) Direct observation of the nanoscale dynamics of membrane lipids in a living cell. *Nature* 457:1159–1163.
3 Fries JR, et al. (1998) Quantitative identification of different single molecules by selective time-resolved confocal fluorescence spectroscopy. *J Phys Chem A* 102(33):6601–6613.
4 Kask P, et al. (1999) Fluorescence-intensity distribution analysis and its application in biomolecular detection technology. *Proc Natl Acad Sci USA* 96:13756–13761.
5 Koppel DE (1974) Statistical accuracy in fluorescence correlation spectroscopy. *Phys Rev A* 10(6):1938–1945.


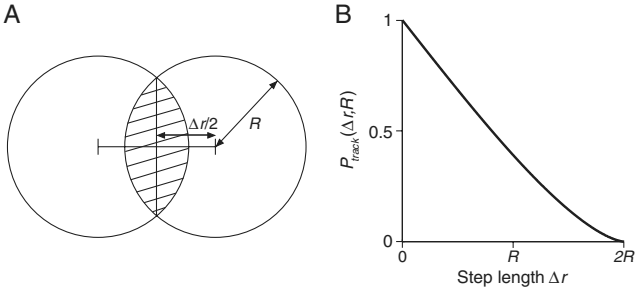


**Fig. S7.** Calculation of the correction factor for a finite observation area $\pi R^2$. We compute the probability $P_{\text{track}}(\Delta r, R)$ of detecting a step of length $\Delta r$ for which both the initial point and the end of the displacement vector lie within the circle of radius $R$. This probability is equivalent to the convolution (overlap integral) of two circles with radius $R$ and center-to-center distance $\Delta r$, as depicted in (*A*). We therefore determine the proportion of the joint area segment to the area of one of the circles. By simple trigonometry, we obtain the expression

$$P_{\text{track}}(\Delta r, R) = \frac{2}{\pi}\arccos\left(\frac{\Delta r}{2R}\right) - \frac{\Delta r \cdot \sqrt{4R^2 - (\Delta r)^2}}{2\pi R^2},$$

which is plotted in (*B*) for $0 \le \Delta r \le 2R$. We correct the probability density $p(\Delta r^2, \Delta t)$ by $1/P_{\text{track}}(\Delta r, R)$ before cumulation and normalization along $\Delta r^2$ to yield the cumulative probability $P(\Delta r^2, \Delta t)$.